Mechanics of Soft Materials (2020) 2: 2
https://doi.org/10.1007/s42558-019-0015-z

ORIGINAL PAPER

Instability and critical pulling rate of tethers in tether extension process using a mathematical model

A. H. Karimi[1] · M. Rahimi[2] · S. Ziaei-Rad[1] · H. R. Mirdamadi[1]

Received: 28 September 2019 / Accepted: 5 December 2019 / Published online: 4 February 2020

Abstract
Cells and organelles are enclosed by a biological membrane called the lipid bilayer membrane. These membranes appear in a variety of complex shapes under certain conditions of the surrounding environment. Shape transformation of lipid bilayers is involved in many cellular processes to perform essential functions. Hence, dynamic behavior of lipid bilayer membranes is one of the important subjects of researches in the last decades. Among different shape transformations of biomembranes, formation of tubes and tethers is quite common in cells and between cells. Tubular networks of the Golgi apparatus and the smooth part of the endoplasmic reticulum and tubes involving cell-cell adhesion are clear examples of formation of tubes. Most of these shape transformations in the cell are carried out by the action of motor proteins of cytoskeleton. In this paper, a mathematical model based on the mechanical properties of fluid bilayer membranes is utilized to study the dynamic behavior of the tether extension process. The dynamic pulling force of the tether extracted by a constant pulling rate is obtained as a function of tether length. The effect of the pulling rates on the dynamic pulling force and shape transformation of bilayer membrane is investigated. By increasing the pulling rate, pearling occurred in the tether. For a specific value of pulling rate called the critical pulling rate, the dynamic pulling force tends to zero and the tether becomes unstable. The effect of material parameters on the critical pulling rate of tethers is also investigated.

Keywords Lipid bilayer membrane · Tether extension process · Critical pulling rate · Instability

1 Introduction

Lipid bilayers are plasma membranes made of two monolayers of lipid molecules and amphiphilic proteins [1, 2]. Lipid molecules consist of two parts, namely, hydrophilic head and hydrophobic tail self-assembled into a bilayer [3, 4]. This polar structure with the hydrophobic core in the center separates the interior from the exterior of cells and organelles, monitoring the passage of ions and other molecules [5].

Due to the chemical and physical state of the bilayer membranes and the external excitations, vesicles can undergo complex morphologies [6, 7]. Various morphologies exhibited by vesicles are usually shown in a diagram called the phase diagram. These stationary shapes that vesicles can get are from stomatocytes and oblates to prolates and pears [8, 9]. Dynamics and shape transformation of membranes are crucial for the role cells and organelles play like budding, endo-, and exocytosis [10].

Bilayer membranes own numbers of mechanical properties of both solids and fluids evaluated by the experimental tests [11, 12]. A wide range of shapes exhibited by vesicles is due to the fluidity and flexibility in bending of bilayer membranes. Therefore, mechanical models can be used to study the behavior of such structures. First, models describing the bending elasticity of membranes were introduced by [13, 14]. Then, the model extended to the bilayer membranes and the effect of stretching elasticity

✉ A. H. Karimi
amir.karimi@me.iut.ac.ir

[1] Department of Mechanical Engineering, Isfahan University of Technology, Isfahan, Iran

[2] Lewis-Sigler Institute for Integrative Genomics, Princeton University, Princeton, USA

was included [15, 16]. Later, tangential mobility of each monolayer was also added in the recent model [17, 18] resulting in inter-monolayer drag and dissipation. Another dissipation mechanism created in fluid bilayer membranes was also considered due to the viscosity of each monolayer in the model. Both dissipation mechanisms produced tangential stress on bilayer.

Among different dynamic procedures and shape transformation of membranes, formation of tubular structures from membranes called tethers is well-known. Tethers are involved in many cellular processes such as inter- or intra-cellular transport [19] and cell-cell adhesion [20, 21]. Tubular networks are also observed in the Golgi apparatus, the smooth part of the endoplasmic reticulum, and the inner membrane of the Mitochondrion [22, 23]. One important in vivo example of tube formation is the action of cytoskeletal motor proteins such as dynein and kinesin [24, 25]. Motor proteins convert chemical energy to pull on the membrane mechanically, move along microfilaments or microtubules created by cytoskeleton, form and elongate the membrane tubes [26, 27]. Membrane tubes can also be formed by in vitro experiments. Tethers are extracted from synthetic vesicles by different techniques like optical tweezer [28] and hydrodynamic flow [29, 30]. Mechanical properties of the bilayer membrane can be measured by these experiments.

From a theoretical point of view, numerous researches were conducted to study the tether extension process and provide a formulation for this problem. In the static state, the tether was considered as a tube pulled out of a planar monolayer membrane under the action of the surface tension on the boundaries and the static pulling force. The radius of the tube and the static pulling force were obtained by minimizing the work done by external and elastic forces which were a function of the bending rigidity and the surface tension [31, 32]. Some researchers directed their attention toward the dynamic behavior of this process. Formulations in this case were provided for a tube [33] or cone [34] like tethers extracted from a planar monolayer membrane by a constant pulling rate. Pearling instability of tubes and tethers under the action of specific parameters is another field of study [35]. Pearling and vesiculation of tubes subjected to osmotic gradients were studied in [36]. It was also shown that electric fields can induce pearling instability in tethers [37].

In this paper, the dynamic behavior of a bilayer membrane in a tether extension process is studied using a mathematical model. A fluid bilayer membrane is utilized in this model consisting of two monolayers sliding on each other. The bending and stretching energy in addition to dissipations due to the viscosity of each monolayer and the inter-monolayer drag are defined for the bilayer membrane. The tether is extracted from a planar bilayer membrane by a constant pulling rate. The dynamic pulling force of the tether is obtained as a function of tether length for different pulling rates. A region of instability is observed during the tether formation depending on the pulling rate. There is a critical pulling rate beyond which the tether becomes unstable. This critical pulling rate depends on the material parameters of the bilayer membrane. The region of instability for bending rigidity, stretching rigidity, and inter-monolayer drag coefficient is introduced. The results of this study will help researchers in conducting experiments.

2 Theory

To study the dynamic behavior of a fluid bilayer membrane, the mathematical model introduced in [18] is utilized. This model is briefly described in this section and the detail information about the formulations is not presented here for the sake of brevity. A lipid bilayer membrane consists of two thin monolayers of lipid molecules as it is depicted in Fig. 1a. Each monolayer is recognized by a surface called the neutral surface representing its mechanics. It is more suitable to define all parameters on the midsurface which is at the distance d from each neutral surface representing the shape of the membrane. The neutral surface and the midsurface are shown in Fig. 1b.

Each point on the midsurface can be specified by the position vector $\mathrm{r} = \mathrm{r}(u^1, u^2, t)$ in the reference frame where u^1, u^2 are the curvilinear coordinated in the surface [38]. The velocity of a point on the midsurface can be obtained by taking time derivative of the position vector. Since the monolayers are capable of sliding on each other, the velocity of a material point on each monolayer and a point on the midsurface are the same in the normal direction but differ in the tangential plane. It can be summarized as follows:

$$V = \frac{d}{dt} r\left(u^1, u^2, t\right) = v + v_n n, v = v^\alpha t_\alpha = \left(v_b\right)^\alpha b_\alpha \tag{1}$$

$$\begin{cases} V^i = v^i + v_n n, v^i = \left(v^i\right)^\alpha t_\alpha = \left(v_b^i\right)^\alpha b_\alpha \\ V^o = v^o + v_n n, v^o = \left(v^o\right)^\alpha t_\alpha = \left(v_b^o\right)^\alpha b_\alpha \end{cases} \tag{2}$$

where V is the velocity of a point on the midsurface consisting of tangential parts (v^α) and a normal component (v_n) in the normal direction (n). V^i and V^o are the velocity of material points on the inner and the outer monolayers, respectively, which are different

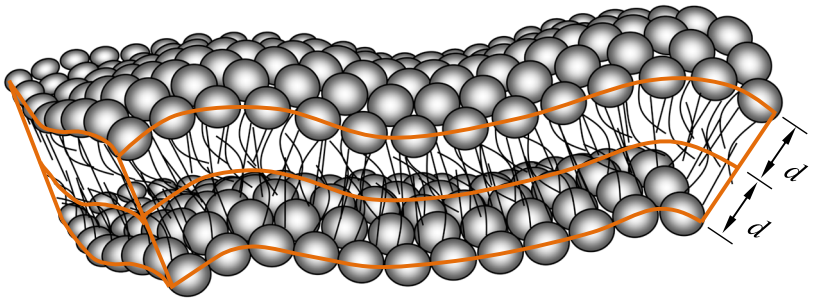

(a) Schematic of a bilayer membrane

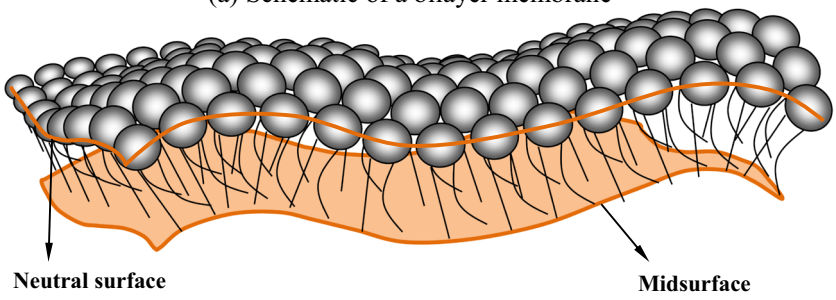

(b) Description of the neutral surface and midsurface

Fig. 1 A lipid bilayer membrane. **a** Schematic of a bilayer membrane. **b** Description of the neutral surface and midsurface

in the tangential plane due to the slippage of the monolayers. $b_\alpha = \partial r/\partial u^\alpha$ is the base vector relative to the curvilinear system which can be normalized as $t_\alpha = b_\alpha/|b_\alpha|$.

2.1 Governing equations

In this section, the governing equations of a fluid bilayer membrane are obtained by taking advantage of an energy approach. In the absence of the inertial forces due to its negligible effect, the power of the system consisting of the rate of the elastic energies and the dissipation functions is minimized to derive the governing equations.

The total elastic energy of a curved membrane consisting of the bending and stretching energy is written as follows:

$$E = E_b + E_s = \int \frac{\kappa}{2}(2H - C_0)^2 \mathrm{d}A + \int \frac{K_s}{2}\left[\left(\frac{\rho^i}{\rho_0} - 1 + 2dH\right)^2 + \left(\frac{\rho^o}{\rho_0} - 1 - 2dH\right)^2\right]\mathrm{d}A \tag{3}$$

The first and the second terms in the right side of Eq. 3 are the bending and stretching energy, respectively. κ and K_s are the bending and stretching modulus, respectively. $2H$ is the mean and C_0 is the spontaneous curvature which is considered zero in this study. ρ^i and ρ^o are the density of the inner and the outer monolayer projected to the midsurface, respectively. ρ_0 is the equilibrium density and is the same for both leaflets. dA is an element of area positioned on the midsurface.

Two main dissipative mechanisms are acting on the fluid bilayer membrane. One is created by the viscosity of each leaflet and the other one is the inter-monolayer drag caused by the slippage of the monolayers. By considering the monolayers as a 2-D Newtonian interfacial fluid and assuming a linear relationship between the drag force and the relative tangential velocity of the monolayers, the dissipation potentials can be written as follows:

$$\begin{cases} W_{\text{visc}} = \frac{1}{2}\int\left\{\lambda\left[\left(S^i\right)^\gamma_\gamma\right]^2 + 2\mu\left(S^i\right)^\beta_\gamma\left(S^i\right)^\gamma_\beta\right\}\ \mathrm{dA} + \frac{1}{2}\int\left\{\lambda\left[\left(S^o\right)^\gamma_\gamma\right]^2 + 2\mu\left(S^o\right)^\beta_\gamma\left(S^o\right)^\gamma_\beta\right\}\ \mathrm{dA} \\ W_{\text{fric}} = \frac{1}{2}\int\mu_f\left|v^o - v^i\right|^2\mathrm{dA} \end{cases} \tag{4}$$

where λ and μ are the shear and dilatational viscosities of the monolayers and μ_f denotes the drag coefficient. $\left(S^i\right)^\beta_\alpha$ and $\left(S^o\right)^\beta_\alpha$ are the rate-of-deformation tensor of the inner and the outer monolayers, respectively, which are as follows:

$$\left(S^i\right)^\beta_\alpha = \frac{1}{2}\left[\left(v^i_b\right)^\beta_{,\alpha} + \left(v^i_b\right)^\alpha_{,\beta}\right] - g^{\alpha\gamma}b_{\gamma\beta}v_n, \left(S^o\right)^\beta_\alpha = \frac{1}{2}\left[\left(v^o_b\right)^\beta_{,\alpha} + \left(v^o_b\right)^\alpha_{,\beta}\right] - g^{\alpha\gamma}b_{\gamma\beta}v_n \tag{5}$$

In Eq. 5, $()_{,\alpha}$ denotes the covariant derivative [38]. $g^{\alpha\gamma}$ is the contravariant metric tensor and $b_{\gamma\beta} = n \cdot \frac{\partial^2 r}{\partial u^\gamma \partial u^\beta}$ is created in the second fundamental form of the midsurface.

The numbers of lipid molecules in the inner and the outer leaflets are $N^i = \int \rho^i dA$ and $N^o = \int \rho^o dA$, respectively. By taking time derivative of these equations, the continuity equations will be obtained as follows, if the number of lipid molecules in both monolayers is constant:

$$\begin{cases} \dfrac{d\mathrm{N}^i}{dt} = \dfrac{d}{dt}\int \rho^i dA = 0 \\ \dfrac{d\mathrm{N}^o}{dt} = \dfrac{d}{dt}\int \rho^o dA = 0 \end{cases} \tag{6}$$

The power functional is the power of the system added by constraints such as volume or area constrains and boundary conditions. It is presented as follows:

$$P = W_{\text{visc}} + W_{\text{fric}} + \dot{E} - \sum_i \lambda_i c_i \tag{7}$$

where λ_i is the multiplier of the i-th constraint (c_i). Constraints are expressed in velocity form as it is used in the power functional.

The governing equations can be obtained by minimizing Eq. 7 with respect to velocities (v^α, v_n, $(v^i)^\alpha$, $(v^o)^\alpha$) and the multipliers.

2.2 Solution

In this section, we turn our attention to the surfaces of revolution. The generating curve is rotated around the z axis and the surface is parametrized by:

$$\begin{cases} r^1(s,\theta,t) = x(s,t)\cos\theta \\ r^2(s,\theta,t) = x(s,t)\sin\theta \\ r^3(s,\theta,t) = z(s,t) \end{cases} \tag{8}$$

where $u^1 = s$, $u^2 = \theta$ are the curvilinear coordinates and the generating curve is in the xz plane.

With the definition of Eq. 8, one can find the tangential and normal velocity of a point on the midsurface as a function of x, z and their time derivative. It is important to note that by using Eq. 8, all the variables are only a function of $u^1 = s$. Also by substituting Eq. 8 into Eq. 1, one can easily find that the tangential velocity of the midsurface and each leaflet has a component only in the s direction which means $v^i = (v^i)^\alpha t_\alpha = v^i t_1$, $v^o = (v^o)^\alpha t_\alpha = v^o t_1$.

The problem is solved numerically by a finite element method taking advantage of B-spline basis functions [39] and the Galerkin method to discretize the governing equations.

Each variable can be decomposed into space and time parts as follows:

$$q(s,t) \approx {}^pN^{q\mathrm{T}}(s)q(t) \tag{9}$$

where ${}^pN^{q\mathrm{T}}(s)$ is a $n_q \times 1$ vector of B-spline basis functions of order p and n_q is the number of control points. $q(t)$ is the vector of time part describing the magnitude of the variable in control points. In this study, $q(s, t)$ is substituted by $x(s, t)$, $z(s, t)$, $v^i(s, t)$, $v^o(s, t)$, $\rho^i(s, t)$, and $\rho^o(s, t)$.

By replacing Eqs. 8 and 9 into Eq. 7 and minimizing the power function, the governing equations are obtained as follows [18]:

$$\begin{cases} D\begin{Bmatrix} \dot{x} \\ \dot{z} \\ \dot{v}^i \\ \dot{v}^o \end{Bmatrix} + C\lambda + f = 0 \\ C^T\begin{Bmatrix} \dot{x} \\ \dot{z} \\ \dot{v}^i \\ \dot{v}^o \end{Bmatrix} = 0 \end{cases} \tag{10}$$

where D and C are functions of x, z called the dissipation and the constraint matrix. λ is a vector containing all the constraint multipliers and f is created by minimization of the elastic energy and is a function of x, z, ρ^i, ρ^o.

Discretizing the continuity equations of the both monolayers results in:

$$\begin{cases} D_{\rho^i}\dot{\rho}^i + K_{\rho^i}\rho^i = 0 \\ D_{\rho^o}\dot{\rho}^o + K_{\rho^o}\rho^o = 0 \end{cases} \tag{11}$$

In which K_{ρ^i} and K_{ρ^o} are functions of $x, z, \dot{x}, \dot{z}, v^i, v^o$.

Equations 10 and 11 are two sets of first-order ODEs which should be solved simultaneously for variables x, z, v^i, v^o, ρ^i, ρ^o. An ODE solver is utilized to solve these equations numerically. In the first step, with the initial values for the shape parameterizations and densities, the velocity variables are calculated from Eq. 10. Then, matrices D_{ρ^i}, D_{ρ^o}, K_{ρ^i}, and K_{ρ^o} which are functions of velocities are computed and the derivatives of densities are calculated from Eq. 11.

3 Results

In order to model the tether pulling out of a giant vesicle, one can model the whole vesicle which is pressurized by an external suction. Another way which is more efficient computationally and utilized in this study is to model the region around the extraction point. Since the vesicle is large enough, this part can be modeled as a disk which means that the generating curve is a line parallel to the x axis as shown in Fig. 2.

To consider the effect of the initial pressure in the vesicle on the disk, we put surface tension on the boundaries of each monolayer (σ^i, σ^o). The surface tension in a thin single membrane can be calculated by the Young-Laplace equation [40] which relates the pressure difference between two sides of a surface to its shape. For a static surface, the relation is $\Delta p = 2H\sigma$ where $\sigma = 2\sigma^i = 2\sigma^o$ can be used for a bilayer membrane. Also, the tangential velocity of the monolayers is set free on the boundaries so that the disk part can exchange mass with the reservoir.

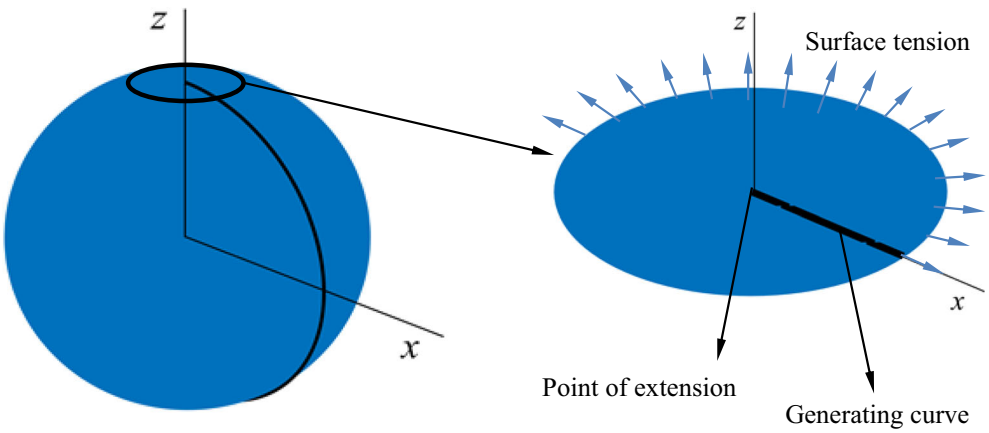

Fig. 2 Generating curve of a disk membrane used to model tether extension procedure

In this study, tether is pulled out from the center of the disk at constant rate $\dot{z}_0$ and the force is measured. This can be added to the governing equations by a constraint where its multiplier corresponds to the force needed to pull the tether out. The basic material parameters of a lipid bilayer membrane are presented in Table 1.

3.1 Static state

Consider the tether pulled out from the bilayer membrane and is held in equilibrium. A simple formulation was presented in literature for this case, modeling the tether as a cylinder of radius r_s and length l. The static pulling force and the radius of the tether in equilibrium state were obtained by minimizing the work done by external force, surface tension, and the elastic forces. These parameters were reported as follows [34]:

$$r_s = \sqrt{\frac{\kappa}{2\sigma}}, f_s = 2\pi\sqrt{2\kappa\sigma} \tag{12}$$

Because of the fact that the curvature of the membrane is higher in the region of tether, the bending energy of the membrane in static state with no spontaneous curvature can be written as follows:

$$\frac{E_b}{\kappa} = \int \frac{1}{2}(2H)^2 \mathrm{dA} \approx \frac{\pi}{r_s} z_0 \tag{13}$$

By substituting the bending modulus from Table 1 and the surface tension is equal to $\sigma = 10^{-5}$N/m into Eqs. 12 and 13, the radius of tether and the pulling force in its static state are obtained and presented in Table 2.

3.2 Dynamic procedure

With the given values in Table 1 and the surface tension ($\sigma = 2\sigma^i = 2\sigma^o = 10^{-5}$N/m), the dynamic behavior of the tether extension process is studied. The normalized pulling force as a function of tether length is obtained for three different values of constant pulling rates $\dot{z}_0$, i.e., 20, 50, and 100μm/s.

As it is observed in Fig. 3a, the dynamic pulling force first grows linearly with the tether length until reaching its maximum value. Then, the dynamic pulling force oscillates about the static value f_s and consequently converges to it. It can be concluded that the shape of the tether converges to a cylinder of radius r_s and length z_0 in a steady state which is the shape of the static state. The maximum value of the dynamic pulling force is the same for the three cases which is $f_{\mathrm{Max}} = 1.131 f_s$. The length of the tether in which this maximum value is occurred is $(z_0)_{\mathrm{Max}} = 0.61\mu$m which is identical for three cases.

After the peak point, the dynamic pulling force decreases and reaches a local minimum. It is shown that the value of local minimum decreases as the pulling rate increases, and therefore, the tether reaches its steady state at higher length. For example, for the first two cases ($\dot{z}_0 = 20, 50\mu\mathrm{m/s}$), the pulling force approaches its static value at the length $z_0 = 0.75\mu$m while for the third case ($\dot{z}_0 = 100\mu\mathrm{m/s}$), this length increases to $z_0 = 7.1\mu$m. This can also be verified by the bending energy of the membrane as a function of tether length which is shown in Fig. 3b. The bending energy of the membrane in the first two cases is almost the same and it grows linearly by tether length after $z_0 = 0.75\mu$m. This is due to the fact that in these two cases, the dynamic pulling force and tether shape approaches its steady state in $z_0 = 0.75\mu$m. In steady state, the tether is similar to a cylinder where the bending energy of the membrane is calculated by Eq. 13 and is a linear function of tether length. The slope of the linear part of the bending energy curve for these two cases is $\pi/r_s = 44.4$ as reported in Table 2. The nonlinear part of the bending energy corresponds to the beginning of the dynamic procedure where the tether is not a cylinder. In the third case, the tether shape reaches its steady state at a higher length of tether. So, its shape deviates from the cylinder of radius r_s which is the shape of the steady state. This leads to the difference between the results of the bending energy for the first two cases and the third case.

There is an important point in Fig. 3c which is a basis of the next section. The total elastic energy of the membrane is depicted versus tether length. By comparing with Fig. 3b, one can find that the effect of the stretching energy in the first two cases is negligible while in the third case, the stretching energy has a great influence on the problem. It seems that in the third case, the

Table 1 Material properties of lipid bilayer membrane [11]

d(m)	κ(N. m)	K_s(N/m)	μ(N. s/m)	λ(N. s/m)	μ_f(N. s/m^3)
1.2×10^{-9}	10^{-19}	0.1	10^{-10}	10^{-7}	10^{8}

Table 2 The radius of the tether and the pulling force in static state

r_s(nm)	f_s(pN)	π/r_s
70.7	8.89	44.4

density of the monolayers deviate significantly from the equilibrium density. For this purpose, the mean normalized density of the outer monolayer is drawn as a function of tether length for the second and the third cases in Fig. 4a.

As it is depicted in Fig. 4a, the mean density of the outer monolayer is close to the equilibrium density for the case $\dot{z}_0 = 50$ μm/s as the stretching energy is negligible. However, for the case $\dot{z}_0 = 100\mu$m/s, the mean density of the outer monolayer deviates considerably from equilibrium density which results in a large stretching energy as illustrated in Fig. 3c. This can also be observed in Fig. 4b where the bending and total elastic energy of the membrane are drawn versus tether length for this case. The maximum stretching energy is $(E_s/\kappa)_{\text{Max}} = 59.27$ which occurred at $z_0 = 1.80\mu$m.

It is important to mention that there is a consistency between the dynamic pulling force of tether and the mean density of the monolayers and consequently the total elastic energy of the membrane diagrams. For the case $\dot{z}_0 = 100\mu$m/s, as the dynamic pulling force decreases after the peak point toward the local minimum point, the density starts to deviate significantly from the equilibrium density and the difference is created between the bending and total elastic energies is growing. The large stretching energy is created in the range of tether length where the dynamic pulling force is smaller than its static value after the peak point. Also, the stretching energy becomes larger as the dynamic pulling force decreases more. Between two diagrams of dynamic pulling force, the one with the lower value of local minimum point has a higher amount of stretching energy.

The question that arises here is that why the stretching energy increases as the dynamic pulling force decreases. The answer to this question leads us to the topic of instability of tethers in tether extension process. The disk membrane used in the problem is in exchange of mass with the rest of the vesicle. In other words, the mass can enter the membrane from the boundaries of the disk. By pulling the center point of the disk, mass enters into the membrane allowing formation of the tether. Therefore, there is a balance between the pulling of the tether and the mass exchange with the rest of the vesicle. When the membrane is pulled out with a higher pulling rate, the tangential velocity of the monolayers increases on the boundaries of the membrane and extra mass enters the membrane. This extra mass causes deviation of the density of the monolayers from the equilibrium density and is the main reason for increasing the stretching energy as shown in Fig. 4. Increase in the density of the monolayers reduces the tension

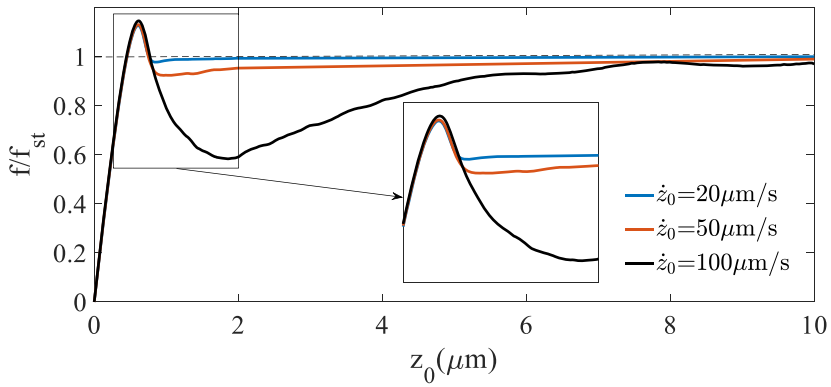

(a) Dynamic pulling force as a function of tether length

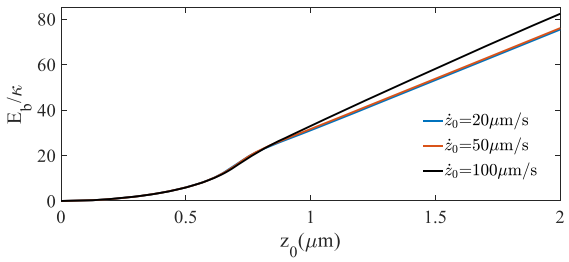

(b) Bending energy as a function of tether length

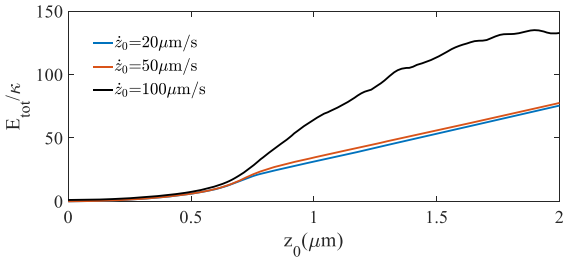

(c) Total energy as a function of tether length

Fig. 3 Dynamic pulling force and elastic energies of the bilayer membrane during tether extension process. **a** Dynamic pulling force as a function of tether length. **b** Bending energy as a function of tether length. **c** Total energy as a function of tether length

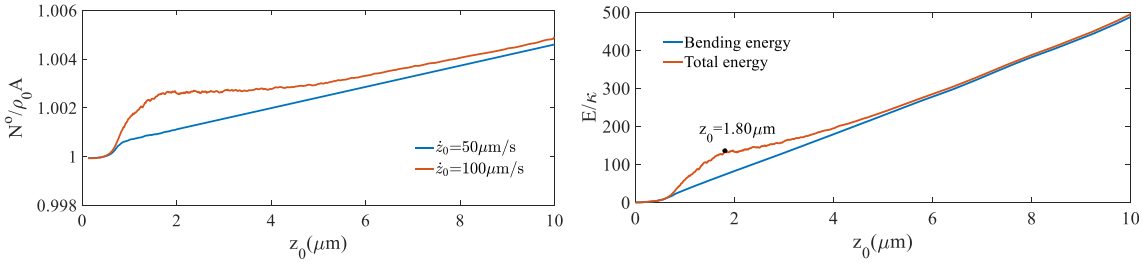

(a) Mean normalized density of the outer monolayer versus tether length

(b) bending and total elastic energy of the membrane for the case $\dot{z}_0 = 100\mu$m/s

Fig. 4 The mean normalized density of the outer monolayer and the energy of the membrane versus tether length.**a** Mean normalized density of the outer monolayer versus tether length. **b** Bending and total elastic energy of the membrane for the case $\dot{z}_0 = 100\mu$m/s

in the membrane and therefore, the dynamic force needed to pull the tether decreases. This is the reason why the dynamic pulling force decreases after its peak point below its static value and reaches the steady state later in the case $\dot{z}_0 = 100\mu$m/s.

3.2.1 Critical pulling rates

By taking another look at Fig. 3a, an idea comes to mind: what will happen by a further increase in the pulling rate of the tether? Is it possible for the dynamic pulling force to decrease and tend to zero? The answer to the last question is positive.

To observe the effect of a further increase in the pulling rate, the center point of the membrane with properties used in the previous section is pulled out with higher pulling rates. The normalized dynamic pulling force as a function of tether length is shown in Fig. 5.

The first two cases are the same as cases in section 3.2.1 while the third case where $\dot{z}_0 = 120\mu$m/s is of importance. It can be seen that the dynamic pulling force decreases below the static value after its peak point in all the cases. In the first two cases, it reaches to a local minimum point and converges to the static value. However, in the third case, a further decrease is observed and the dynamic pulling force intersects with the horizontal axis. This can be expressed that there is no force needed to pull out the

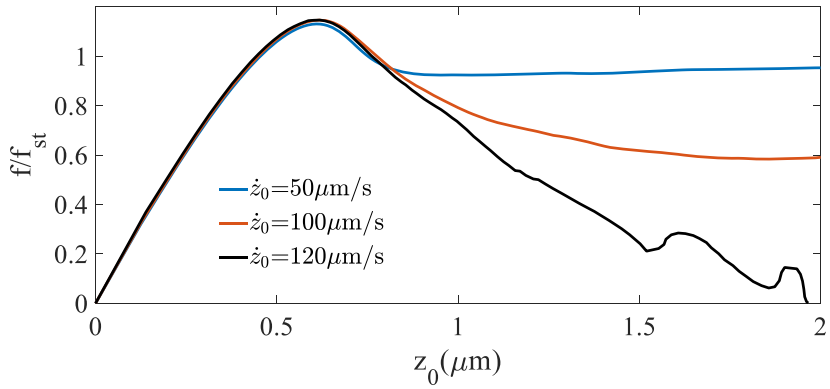

(a) Dynamic pulling force as a function of tether length

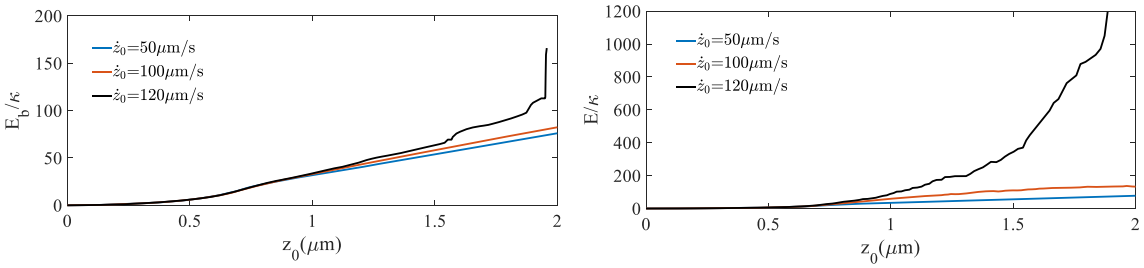

(b) Bending energy as a function of tether length

(c) Total energy as a function of tether length

Fig. 5 Dynamic pulling force and elastic energies of the bilayer membrane during tether extension process. **a** Dynamic pulling force as a function of tether length. **b** Bending energy as a function of tether length. **c** Total energy as a function of tether length

tether at a constant pulling rate describing instability of the tether. In other words, negative values of dynamic pulling force determine the region of instability of the tether extension problem.

It can be concluded that by increasing the pulling rate of the tether, the dynamic pulling force decreases more and approaches to zero. For a certain value of pulling rate, the dynamic pulling force does not converge to static value and it tends to zero. This value of the pulling rate in which the dynamic pulling force tends to zero is called the critical pulling rate. Beyond this value, the tether does not reach the steady state and becomes unstable.

With the description provided in the previous paragraph about the decrease in the dynamic pulling force, one can find the reason of instability. Consider the tether pulled out with a critical pulling rate. The extra mass entering into the disk membrane from the rest of vesicle reduces greatly the tension in the membrane causing a reduction of dynamic pulling force. This means that the balance between the pulling force and the entering mass is not kept and the tether becomes unstable. Therefore, it is expected to see a larger deviation of density from the equilibrium density for the monolayers and consequently divergence in the stretching energy. This is depicted in Fig. 5c where the stretching energy is growing fast. The bending energy of the membrane also increases as the tether becomes unstable and the membrane shape is transformed into a highly curved shape.

In order to see the effect of the pulling rate on the shape of the tether, shape transformation of the membrane is obtained for these three cases, namely $\dot{z}_0 = 50, 100, 120 \mu\mathrm{m/s}$ and shown in Fig. 6.

As it is observed in Fig. 6a, there is a relation between the shape transformation of the tether and the dynamic pulling force. For example, in the case $\dot{z}_0 = 50\mu\mathrm{m/s}$, from the moment the tether is formed, its shape is close to a cylinder with static radius of r_s but with varying length. This is due to the fact that the dynamic pulling force approaches to the static value immediately after its peak point.

In the second case $\dot{z}_0 = 100\mu\mathrm{m/s}$, there is a difference between the dynamic pulling force and its static value after the peak point. Therefore, the shape of the tether deviates from a cylinder with radius r_s. This can be seen in Fig. 6a where the neck of the tether has the lowest radius. The most important point in the shape of the tether in this case is creation of pearls along the length of the tether. These pearls are better shown in Fig. 6b. The reason why these shapes are formed is the extra mass which is entering into the disk. The extra mass extends the surface and consequently increases the surface area of the tether. Increase in the surface area is caused by creation of pearls. Since pearls are curved shapes, the mean curvature of the membrane increases. This will affect the bending energy and can be verified by Fig. 3b in which the bending energy of membrane for the case $\dot{z}_0 = 100\mu\mathrm{m/s}$ increases in comparison with other cases.

The curvature of the pearls increases for the case $\dot{z}_0 = 120\mu\mathrm{m/s}$ before the tether becomes unstable as it is clearly shown in Fig. 6a. Also, the number of pearls increases in comparison to cases with lower $\dot{z}_0$. This is due to the fact that the higher extra mass requires larger surface area in this case. This can also be related to the dynamic pulling force diagram, too. It is observed that when the dynamic pulling force approaches to zero, pearls are clearer and the number of them increases. The lower is the dynamic pulling force, the higher is the number of pearls in the tether.

It is concluded that pearling of tethers in the tether extension process is a prelude to the instability of them. In this stage, the shape of tethers deviates from the steady-state shape which is a cylinder and then pearls before becoming unstable. The most important note is that the formulation used in the literature for the tether extension process is feasible when the tether is going to pearl and the dynamic pulling force deviates from its static value. Modeling the tether as a cylinder or cone is no longer capable of observing this procedure. A model like the one introduced in [18] is able to completely describe the dynamic features of the bilayer membranes and to predict the correct shape transformations in tethers.

3.2.2 The effect of material parameters

By definition of instability region for tethers, it seems that the material parameters of the bilayer membrane may have an influence on the critical pulling rate. The material parameters are the bending and stretching moduli, the shear and dilatational viscosities, and the drag coefficient. In order to study the effect of these parameters on the critical pulling rate of tethers, the values given in Table 1 are considered as the basic values. In each step, the critical pulling rate of the tether is obtained for different values of one parameter while other parameters are kept fixed. In this case, one can investigate the effect of each parameter separately on the critical pulling rate. Different values of each parameter are chosen from the range where it varies for the bilayer membranes.

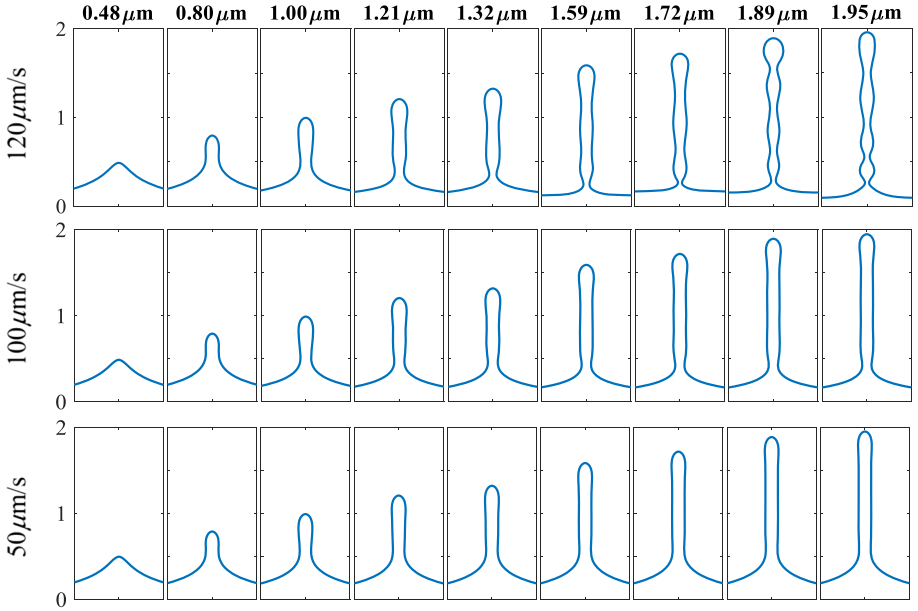

(a) Shape transformation with three different values of pulling rate

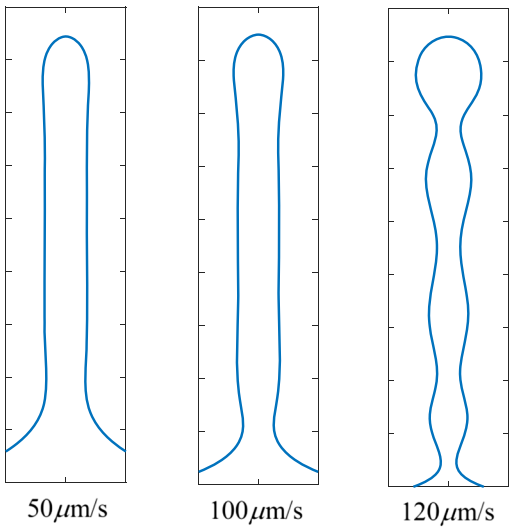

(b) Closer look to the tether shapes at the length of 1.89μm

Fig. 6 Shape transformation of the membrane in tether extrusion process. **a** Shape transformation with three different values of pulling rate. **b** Closer look to the tether shapes at the length of 1.89μm

It was observed that the critical pulling rate is greatly affected by changing the values of the bending and stretching moduli and the drag coefficient. On the contrary, the effect of the shear and dilatational viscosities on the critical pulling rate is negligible. This will prove that the bending and stretching energies and the drag force due to the slippage of monolayers are the dominant mechanisms in the shape transformation and the dynamic procedure of the tether extension process. The effect of bending modulus, stretching modulus, and drag coefficient on the critical pulling rate is shown in Fig. 7.

As it is depicted in Fig. 7a, the critical pulling rate increases by the increase in the bending modulus. This can be explained by the relation between the bending energy and the pearling of the tether. By increasing the bending modulus, there is a stronger resistance in membrane for creation of curved shapes. Therefore, a greater pulling rate is needed for pearls to be formed as they increase the curvature in the tether. In the similar analysis, increasing the stretching modulus reduces the deviation of the density of the monolayers from the equilibrium density. In this case, the pulling rate should increase to bring in the extra mass needed to form the pearls from the rest of the vesicle and the critical pulling rate increases. However, the results are different for the drag coefficient. By increasing this parameter, the difference between the tangential velocities of the inner and the outer monolayers is

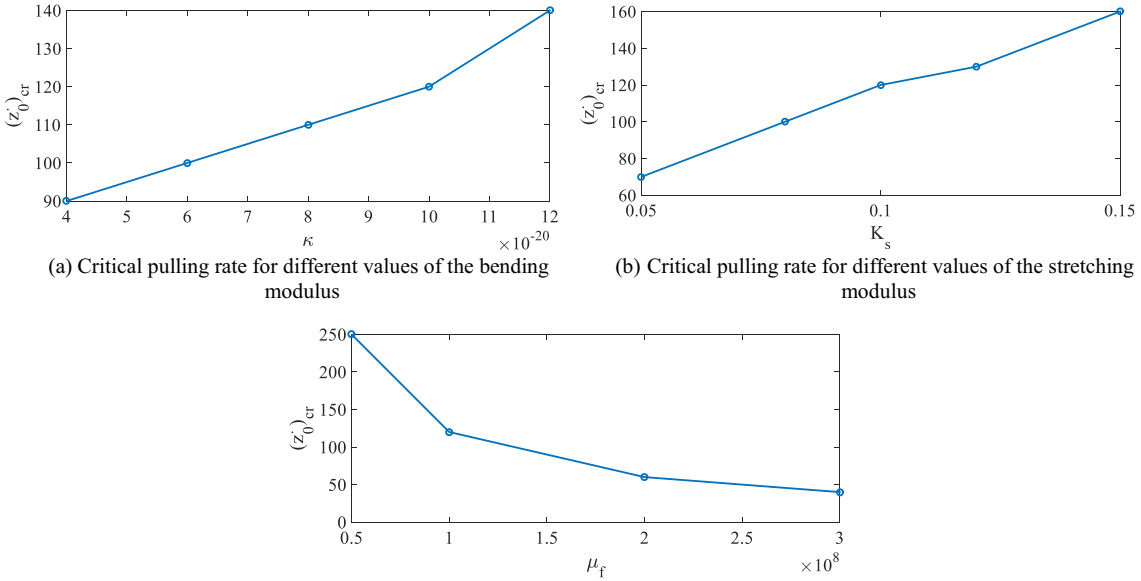

(a) Critical pulling rate for different values of the bending modulus

(b) Critical pulling rate for different values of the stretching modulus

(c) The critical pulling rate for different values of the drag coefficient

Fig. 7 The effect of material parameters on the critical pulling rate. **a** Critical pulling rate for different values of the bending modulus. **b** Critical pulling rate for different values of the stretching modulus. **c** The critical pulling rate for different values of the drag coefficient

decreased and the bilayer membrane acts as a monolayer. Hence, the amount of the extra mass entering the tether increases and the tether becomes unstable at lower pulling rates. The critical pulling rate is reduced by increasing the drag coefficient.

4 Conclusions

In this paper, the dynamic behavior of fluid lipid bilayer membranes in the tether extension process was studied using a continuum model. The elastic energy and the dissipation functions are the mechanisms acting on the bilayer membrane in this model. The study was focused on the tether extension process. A planar bilayer membrane was considered to model the region of a giant vesicle around the extraction point. The tether was extracted on this membrane by a constant pulling rate and the dynamic pulling force was obtained as a function of tether length. It was observed that the dynamic pulling force is decreased after its peak point to reach a local minimum value and then converges to its static value.

Next, the effect of pulling rate was studied. By increasing the pulling rate, the dynamic pulling force deviated more from its static value. In this case, the stretching energy increased considerably due to entrance of mass to the tether from the rest of the vesicle. By further increasing the pulling rate, the local minimum point approached to zero. Due to the extra mass entering the tether, it underwent pearling. It was shown that by approaching the dynamic pulling force to zero, pearls are formed in shapes with higher curvature. At a specific pulling rate called the critical pulling rate, the dynamic pulling force reached to zero which made the tether unstable. The negative values of the dynamic pulling force were introduced as the region of instability in the tether extension process. In the final step, the effect of material parameters of the bilayer membrane on the critical pulling rate was investigated. It was shown that the change in the bending and stretching moduli and the drag coefficient will greatly affect the critical pulling rate of tether while the effect of the shear and dilatation viscosities are negligible.

References

1. Murate, M., Kobayashi, T.: Revisiting transbilayer distribution of lipids in the plasma membrane. J. Chem. Phys. Lipids. **194**, 58–71 (2016)
2. Sackmann, E.: Biological membranes architecture and function. J. Struc. Dyn. Membr. **1**, 1–63 (1995)
3. McNaught, A.D., McNaught, A.D.: Compendium of Chemical Terminology, vol. 1669, (1997) **Blackwell Science Oxford**
4. Voet, D.: Fundamentals of Biochemistry Life at the Molecularlevel, vol. 849, 6th edn. John Wiley & Sons (2012)
5. Johnson, A., Lewis, J.: Molecular Biology of the Cell, 4th edn. Garland Science, New York (2002)
6. Döbereiner, H., Käs, J., Noppl, D., Sprenger, I., Sackmann, E.: Budding and fission of vesicles. Biophys. J. **65**(4), 1396–1403 (1993)

7. Käs, J., Sackmann, E.: Shape transitions and shape stability of giant phospholipid vesicles in pure water induced by area-to-volume changes. Biophys. J. **60**(4), 825–844 (1991)
8. Seifert, U., Berndl, K., Lipowsky, R.: Shape transformations of vesicles: phase diagram for spontaneous-curvature and bilayer-coupling models. J. Phys. Rev. A. **44**(2), 1182 (1991)
9. Seifert, U., Lipowsky, R.: Morphology of vesicles. In: Handbook of biological physics, vol. 1, pp. 403–464 (1995)
10. Svetina, S.: Vesicle budding and the origin of cellular life. J. ChemPhysChem. **10**(16), 2769–2776 (2009)
11. Dimova, R., Aranda, S., Bezlyepkina, N., Nikolov, V., Riske, K.A., Lipowsky, R.: A practical guide to giant vesicles. Probing the membrane nanoregime via optical microscopy. J. Phys. Condens. Matter. **18**(28), S1151–S1176 (2006)
12. Wang, J.H.-C., Thampatty, B.P.: An introductory review of cell mechanobiology. J. Biomech. Model. Mechanobiol. **5**(1), 1–16 (2006)
13. Helfrich, W.: Elastic properties of lipid bilayers: theory and possible experiments. J. Z. Naturforsch. C. **28**(11–12), 693–703 (1973)
14. Deuling, H., Helfrich, W.: The curvature elasticity of fluid membranes: a catalogue of vesicle shapes. J. Physique. **37**(11), 1335–1345 (1976)
15. Evans, E.A.: Bending resistance and chemically induced moments in membrane bilayers. Biophys. J. **14**(12), 923–931 (1974)
16. Seifert, U.: Configurations of fluid membranes and vesicles. J. Adv. Phys. **46**(1), 13–137 (1997)
17. Rahimi, M., Arroyo, M.: Shape dynamics, lipid hydrodynamics, and the complex viscoelasticity of bilayer membranes. J. Phys. Rev. E. **86**(1), 011932–011946 (2012)
18. Karimi, A., Mirdamadi, H., Ziaei-Rad, S.: Mathematical modeling of dynamic behavior of fluid bilayer membranes under the effect of density asymmetry. J. Theor. Biol. 330–344 (2018)
19. Aubertin, K., Tailleur, J., Wilhelm, C., Gallet, F.: Impact of a mechanical shear stress on intracellular trafficking. J. Soft Matter. **13**(31), 5298–5306 (2017)
20. Sackmann, E., Smith, A.-S.: Physics of cell adhesion: some lessons from cell-mimetic systems. J. Soft Matter. **10**(11), 1644–1659 (2014)
21. Schmitz J, Gottschalk K-EJSM (2008) Mechanical regulation of cell adhesion. 4 (7):1373–1387
22. Mollenhauer, H., Morré, D.J.: The tubular network of the Golgi apparatus. J. Histochem. Cell Biol. **109**(5–6), 533–543 (1998)
23. Waterman-Storer, C.M., Salmon, E.: Endoplasmic reticulum membrane tubules are distributed by microtubules in living cells using three distinct mechanisms. J. Curr. Biol. **8**(14), 798–807 (1998)
24. Kolomeisky, A.B.: Motor proteins and molecular motors: how to operate machines at the nanoscale. J. Phys. Condens. Matter. **25**(46), 463101 (2013)
25. TyleráMcLaughlin, R.: Collective dynamics of processive cytoskeletal motors. J. Soft Matter. **12**(1), 14–21 (2016)
26. Borghi, N., Brochard-Wyart, F.: Tether extrusion from red blood cells: integral proteins unbinding from cytoskeleton. Biophys. J. **93**(4), 1369–1379 (2007)
27. Hirokawa, N.: Kinesin and dynein superfamily proteins and the mechanism of organelle transport. J. Sci. **279**(5350), 519–526 (1998)
28. Waugh, R.E.: Surface viscosity measurements from large bilayer vesicle tether formation. II. Experiments. Biophys. J. **38**(1), 29–37 (1982)
29. Raucher, D., Sheetz, M.P.: Characteristics of a membrane reservoir buffering membrane tension. Biophys. J. **77**(4), 1992–2002 (1999)
30. Kremer, S., Campillo, C., Quemeneur, F., Rinaudo, M., Pepin-Donat, B., Brochard-Wyart, F.: Nanotubes from asymmetrically decorated vesicles. J Soft Matter. **7**(3), 946–951 (2011)
31. Brochard-Wyart, F., Borghi, N., Cuvelier, D., Nassoy, P.: Hydrodynamic narrowing of tubes extruded from cells. J Proc. Natl. Acad. Sci. **103**(20), 7660–7663 (2006)
32. Powers, T.R., Huber, G., Goldstein, R.E.: Fluid-membrane tethers: minimal surfaces and elastic boundary layers. J. Phys. Rev. E. **65**(4), 041901 (2002)
33. Derényi, I., Jülicher, F., Prost, J.: Formation and interaction of membrane tubes. J. Phys. Rev. Lett. **88**(23), 238101 (2002)
34. Rossier, O., Cuvelier, D., Borghi, N., Puech, P., Derényi, I., Buguin, A., Nassoy, P., Brochard-Wyart, F.: Giant vesicles under flows: extrusion and retraction of tubes. J. Langmuir. **19**(3), 575–584 (2003)
35. Derényi, I., Koster, G., Van Duijn, M., Czövek, A., Dogterom, M., Prost, J.: Membrane nanotubes, pp. 141–159. Controlled nanoscale motion. Springer, In (2007)
36. Sanborn, J., Oglęcka, K., Kraut, R.S., Parikh, A.N.: Transient pearling and vesiculation of membrane tubes under osmotic gradients. J. Faraday Discuss. **161**, 167–176 (2013)
37. Sinha, K.P., Gadkari, S., Thaokar, R.M.: Electric field induced pearling instability in cylindrical vesicles. J. Soft Matter. **9**(30), 7274–7293 (2013)
38. Sokolnikoff, I.S.: Tensor Analysis: Theory and Applications, 2nd edn. Wiley (1954)
39. Piegl, L., Tiller, W.: The NURBS Book, 2nd edn, (1997) **Springer Science & Business Media**
40. Drioli, E., Giorno, L.: Comprehensive Membrane Science and Engineering: Basic Aspects in Membrane Preparation and their Transport Phenomena. Elsevier Science (2010)

Publisher's note